Power-Hardware-in-the-Loop Validation of Air-Source Heat Pump for Fast Frequency Response Applications

Ruihao Song[1], Anurag Mohapatra[2], Thomas Hamacher[3], and Vedran S. Perić[4]
Munich Institute of Integrated Materials, Energy, and Process Engineering
Technical University of Munich
Garching, Germany

***Abstract*— This paper presents a standard power-hardware-in-the-loop testing platform to simulate detailed air-source heat pump dynamics based on well-established modeling knowledge. Distributed air-source heat pumps can be potentially used for fast frequency response. However, using air-source heat pumps for rapid modulation cannot be based on the current assumptions of linear speed-power transient characteristics developed for low-speed temperature control applications. Customized setups with experimental validation options are needed to design the new fast frequency response compatible heat pump controllers. Most power system laboratories struggle to build a customized air-source heat pump, which hinders research progress. The proposed platform is relatively universal, can fit different heat pumps with minor modifications, and can be implemented on standard PHIL emulators in power system laboratories. Emulation results, real-time implementation details, and model complexity metrics are presented to assist in the transference of the setup to other laboratories.**

***Index Terms*—air-source heat pump, demand-side response, dynamic modeling, power-hardware-in-the-loop, fast frequency response.**

I. INTRODUCTION

A. Backgrounds

In the ongoing efforts to curtail greenhouse gas emissions, there is a growing momentum towards electrifying heating in residential structures using air-source heat pump (ASHP) technology [1]. This transition to ASHPs results in tighter power and heating systems integration, enabling combined operations that enhance efficiency and resilience. The fast-responding potential of distributed ASHPs presents numerous opportunities for improving power grid performance by allowing them to operate in high-speed demand-side response (HSDSR) mode for fast frequency response (FFR) ancillary services [2][3]. Thus, the inertia of the power grid can be enhanced, and the expenditure associated with FFR battery systems can be reduced. HSDSR feature is highly demanding on transient performance and requires careful experimental validation. Unfortunately, specialized sector-coupling equipment such as ASHPs are generally unavailable in default power system laboratories, and commercial ASHPs are very expensive and poor in terms of customization capability. Therefore, handling the ASHP equipment shortage problem in power system laboratories is critical before the later FFR controller design stage.

Power Hardware-In-The-Loop (PHIL) experiments are typically carried out to safeguard the electrical grid against the unpredictable behaviors of physical devices under test. However, PHIL systems offer the unique capability to function as "virtual equipment" via dynamic electrical emulation, which has become increasingly popular for sector coupling research [4][5][6]. This innovative approach uses well-accepted physics-based dynamic modeling techniques to determine the virtual equipment's grid-interfacing current, making it adaptable to an extensive range of working conditions and equipment configurations [7]. The generated current reference is then executed by PHIL emulators, effectively mimicking the actual equipment behavior. As a result, from the grid's standpoint, the distinction between actual and virtual equipment becomes indiscernible. Within this context, PHIL is a pivotal technology in overcoming hardware constraints while developing ASHP-based FFR services. Nevertheless, the cornerstone of creating effective virtual equipment lies in dynamic modeling. Since PHIL experiments operate in real-time, developing an HSDSR-compatible ASHP model poses a significant challenge. It necessitates a balance between dynamic accuracy and computational burden.

Despite the growing awareness of the pivotal role of ASHPs, current ASHP models exhibit notable deficiencies in accurately capturing the non-linear power transient characteristics needed by designing HSDSR control, thereby obstructing the utilization of their flexibility potentials. The physical structure of a typical distributed ASHP is shown in Fig. 1, where the system can be divided into electrical and thermal subsystems. On the one hand, most ASHP models used in electrical power systems research are either static or quasi-static, primarily designed for hourly simulation and optimal power-flow calculations. Existing dynamic models often rely on constant linear time-invariant systems to represent both electrical and thermal subsystems in a lumped manner, which fails to capture the non-linear behavior in HSDSR scenarios accurately [8]. On the other hand, in the area of compression-based refrigeration systems, well-established modeling methodologies exist for the

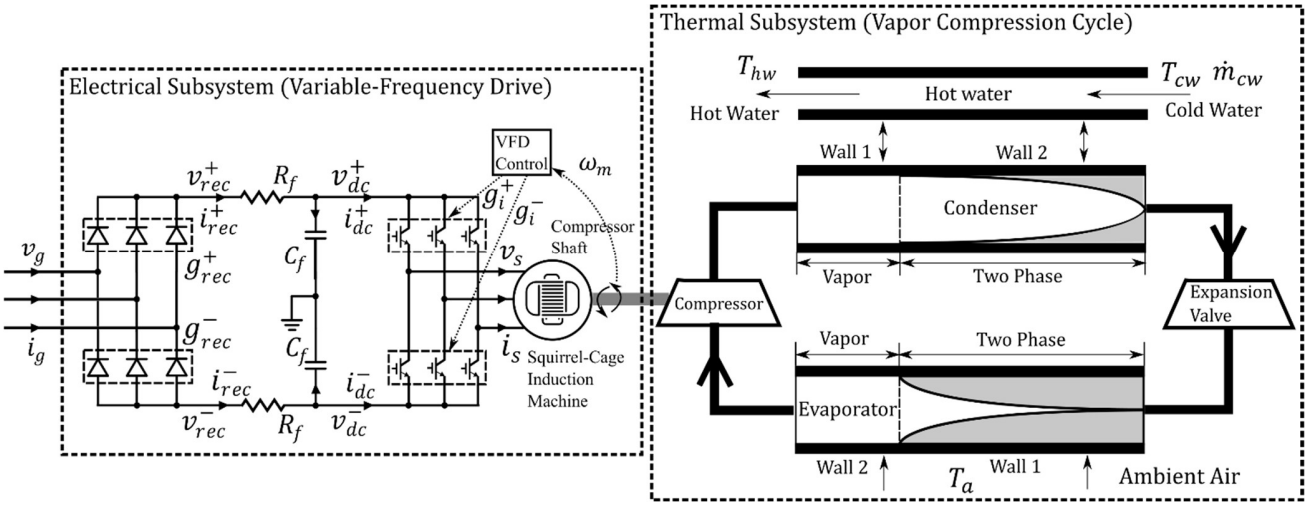

Fig. 1. Physical structure of a typical distributed ASHP (see Appendix for the nomenclature).

non-linear dynamics of the thermal subsystem [9][10][11] in ASHPs. Yet, the electrical subsystem is neglected as the focus of the study is not electrical power.

B. Contributions

This paper proposes a PHIL solution that can emulate the non-linear transient behaviors of distributed ASHPs based on fundamental physics and mathematics. We summarize our contributions as follows:

- The developed model is a multi-physics model that incorporates methods that are well-validated in the known literature.
- We used one case study (15 kW, air-to-water type, R134a refrigerant) to show that the developed ASHP model has an acceptable computational burden and can be deployed and simulated in real-time at kHz rate.
- The developed model can run in a standard PHIL platform [12][6] for experiments on an active distribution grid.

The rest of this paper is organized as follows. In section II, we describe the reason for selecting specific modeling methods. In section III, we introduce the complete PHIL implementation process of the constructed model. In section IV, we show the experimental results in our laboratory environment. Finally, we give the conclusion of this paper in section V.

II. MODELING METHODS

Currently, commercially available modules are designed for maintaining a designated supply water temperature. Therefore, the modulation speed of the variable-frequency drive (VFD) is kept slow as output temperature control does not require rapid modulation. In this context, the non-linear characteristics of the refrigerant circulation system are covered by the slow ramping modulation, thus creating a phenomenon of linear speed-power response characteristics among all working conditions. For example, we tested the speed-power step response of a 4 kW distributed ASHP (WOLF MONOBLOCK) in our laboratory at different working conditions, and the results shown in Fig. 2 suggest linear characteristics, which can justify a transfer function model. However, challenges emerge if the slow ramping style of modulation is insufficient for the application case, such as FFR services.

In the context of FFR, the modulation speed limit of modern ASHPs needs to be removed, and the response will be non-linear at different working conditions. Besides, HSDSR has a harsher transient performance requirement regarding oscillation and stability, as a poorly tuned controller can lead to grid instability. To study how to implement HSDSR on ASHPs, we must carefully model all necessary non-linear behaviors to ensure a feasible controller design. In this paper, we propose to develop a standard ASHP model structure for FFR applications, and the goals are listed as follows.

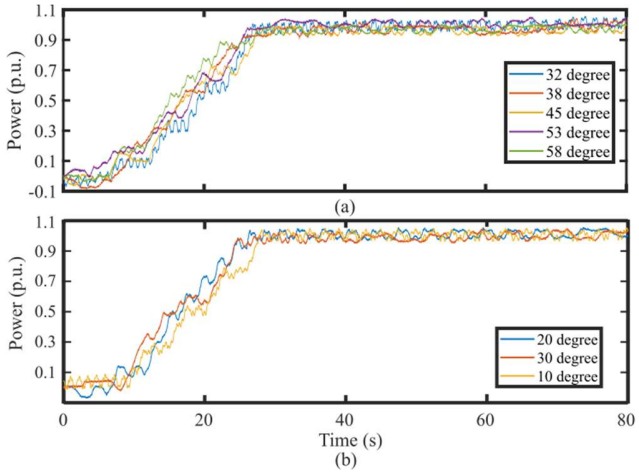

Fig. 2. Speed-power response characteristics of a typical commercial ASHPs (normalized): (a) at different cold water temperatures; (b) at different air temperatures.

TABLE I. EXISTING MAINSTREAM MODELS FOR ELECTRICAL AND THERMAL SUBSYSTEMS FROM THE LITERATURE BASE

Electrical Subsystem	Machine Speed	Grid-side current	Computation
Transfer function	Accurate	N/A	Low
KCL/KVL + switching function [13]	Accurate	Less accurate for the current noise profile	Medium
KCL/KVL + detailed switching	Accurate	Accurate	High

Thermal Subsystem	Mechanical load	Internal states	Computation
Single-phase flow model [14]	Less accurate in both dynamics and steady states	N/A	Low
Hammerstein-Wiener model [15]	Less accurate in dynamics, accurate in steady-states	N/A	Low
Moving boundary model [9][10][11]	Accurate	Less accurate with lumped variables	Medium
Finite volume model [16][17]	Accurate	Accurate	High

- The model should be relatively universal and match different ASHPs from simple parameter tuning.
- The model should be physics-based and reflect the ASHP power response non-linearity at different working conditions.
- The model should be computationally tractable and be deployed in real-time for HIL and PHIL tests.
- All used modeling methods should originate from the previously validated literature.

We separate the ASHP model into electrical and thermal subsystems to reduce the computational burden due to their different transient rates. Table I lists all mainstream methods for the electrical and thermal subsystems separately. The electrical VFD and its modeling are standardized in the power system area, and the differences are only in the level of detail. As we are not interested in the detailed noise profile of the grid-side current, we adopt the KCL/KVL plus switching-function level to model the VFD system [13].

For the thermal subsystem, the choice is between the moving boundary model and the finite volume model because we need an accurate description of mechanical load power transients, which are predominately determined by pressures in the evaporator and condenser. The finite volume method is more precise in refrigerant temperature and specific enthalpy spatial distribution in the condenser and evaporator. Still, that information has little value for the HSDSR controller application. Additionally, one can note that the computational effort needed for the moving boundary model is significantly lower than the finite volume model. A comprehensive comparison between these two modeling methods is done for a 300 kW R134a chiller [16]. The authors mentioned that the moving boundary model executed about three times faster than the finite volume model while maintaining nearly identical accuracy in steady-state and trainset estimations, as shown in Fig. 3. Based on the provided information, the optimal choice is the moving boundary method for the thermal subsystem.

III. PHIL IMPLEMENTATION

A. Model building

The detailed model structure is shown in Fig. 4, and all the fundamental equations for model programming can be found in the Appendix. The electrical subsystem requires the mechanical load power from the thermal subsystem to calculate the load torque on the machine shaft. In contrast, the thermal subsystem requires the shaft speed to calculate the mechanical load power; therefore, the two subsystems are coupled. The overall model input is the speed modulation signal, grid-side voltage waveform, working condition measurements, and superheat reference for the thermal expansion valve. The model output contains but is not limited to grid-side current waveform, mechanical load power, and heated water temperature.

The electrical subsystem is straightforward to construct as the modeling process is already standardized. We chose Matlab/Simulink as the platform to establish the electrical subsystem because it is widely used in power system research areas. We make the model based on the typical physical structure described in Fig. 1a with standard components in the Simscape Specialized Power System Library. Then, we summarize all components with mathematical equations to reduce the computational effort.

The thermal subsystem is relatively complicated to build compared with the electrical subsystem. To model the non-linear flow in the single-cycle refrigerant circulation system, at least mass and energy conservation partial differential equation (PDE) systems need to be solved along the axial direction of the pipe. The moving boundary method simplifies the PDE systems into ordinary differential equation (ODE) systems by dividing the non-linear flow region into length-variant zones where each represents a specific refrigerant state, such as vapor and two-phase mixture zones. This results in a high-order ODE system with coefficients related to media thermal dynamic properties. Modelica environment (Dymola) is the suitable platform to build such systems for the following two reasons. Firstly, it can solve complex ODE systems without manually combining and arranging all equations. Secondly, it has standard refrigerant media libraries that can work as look-up tables to extract the necessary thermal dynamic property coefficients during real-time model calculation.

B. Model deployment

Considering that Matlab/Simulink has better compatibility with standard PHIL setups, we packaged the thermal subsystem model in Dymola with S-function (Dymola block) and coupled these two subsystems on Simulink. This paper uses The Euler solver for both subsystems to lower the computational burden. We must select appropriate computation frequencies for both subsystems to deploy the combined model into the target real-time environment. Choosing a value for the electrical subsystem first is suggested as the non-linear current calculation is more sensitive to the computational frequency.

We simulate the electrical subsystem without the thermal subsystem (constant load torque) at several frequencies, as shown in Fig. 5 and Table II for time and frequency domain, respectively. The results suggest that the lower threshold to keep a decent accuracy is roughly 8 kHz, while the upper threshold is flexible based on the concerned main harmonic bandwidth. In this paper, 10 kHz is selected for the electrical subsystem.

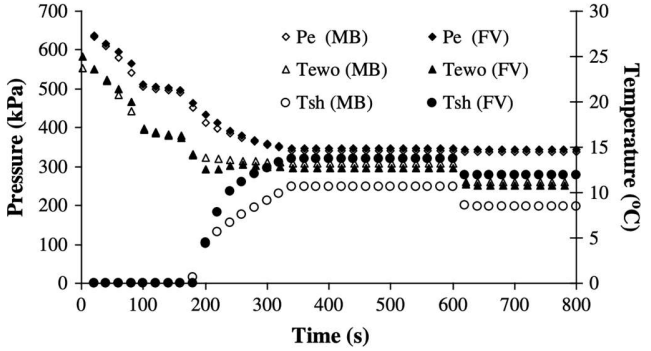

Fig. 3. Finite volume v.s. Moving boundary methods, start-up, and load-change transients [16].

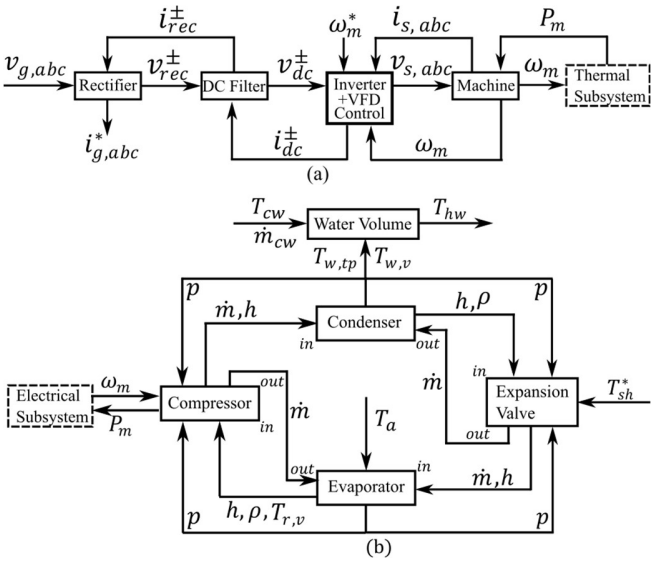

Fig. 4. Model structure of the proposed model (see Appendix for the nomenclature): (a) electrical subsystem; (b) thermal subsystem.

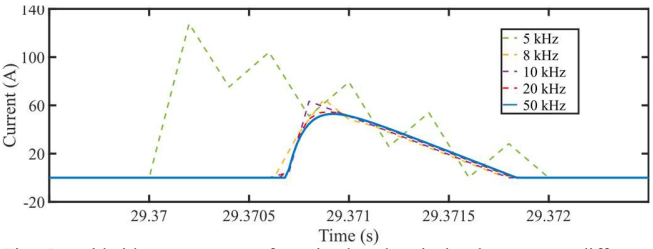

Fig. 5. Grid-side current waveform in the electrical subsystem at different execution frequencies.

TABLE II. MAIN COMPONENTS OF GRID-SIDE CURRENT IN FREQUENCY DOMAIN UNDER DIFFERENT MODEL EXECUTION FREQUENCIES

	Funda.	3	5	7	9	11	13
50 kHz	7.098	6.913	6.553	6.042	5.411	4.697	3.946
20 kHz	7.099	6.917	6.564	6.063	5.443	4.742	4.003
10 kHz	7.08	6.908	6.574	6.098	5.506	4.835	4.124
8 kHz	7.109	6.932	6.587	6.097	5.492	4.808	4.089
5 kHz	9.328	8.728	7.615	6.15	4.536	2.997	1.761

We tend to choose a slower frequency for the thermal subsystem as the thermal dynamics of ASHP are significantly slower than those of its electrical peers. The combined model has a risk of instability if the frequency for the thermal subsystem is too low, while the model can also exceed real-time capacity if it is too high. Therefore, we choose to deploy it at roughly the minimum frequency to ensure model stability, which is 200 Hz with our parameter set. For other parameter sets, the appropriate frequency can be obtained by simulation tests in the Simulink environment.

After fixing the computational frequencies, both subsystems should be compiled and loaded in the real-time environment through C code DLL files. The execution priority should be configured as thermal over electrical subsystems to ensure a smooth start-up. The mechanical speed ω_m and load power P_m should be exchanged between two subsystems through clocked channels.

C. PHIL configuration for the virtual heat pump

The proposed ASHP PHIL emulation platform is used for validating specially designed HSDSR controllers in a realistic grid environment, as shown in Fig. 6a. The developed model is deployed on a NI-PXIe-8880 real-time calculator (Fig. 6b), which runs on PharLap and interfaces with the host PC through the Veristand platform. The calculation result, which is the grid-interfacing current of the virtual heat pump, is sent as a set-point to the Egston (Fig. 6c) COMPISO System Unit (CSU) for execution. During the HSDSR control validation experiment, the controller under test (with the PLL) reads voltage details at the local bus and current shaft power of the virtual ASHP and injects the control signal ω_m^* to the proposed virtual heat pump system. This setup establishes a realistic ancillary service test environment. Although the equipment supplier could be diverse, the mentioned application scenario can be migrated to most power system laboratories, generally equipped with real-time simulators and PHIL test beds. Details on our lab specifications and their universality can be found in [6].

IV. RESULTS

A. Advantages over traditional models

In this subsection, we aim to show that the proposed modeling methodology for ASHP systems offers superior performance to traditional modeling techniques in designing HSDSR controllers. The evaluation of model suitability for FFR services necessitates focusing on power step response analysis instead of the conventional assessment through half-minute or minute-level ramping. This shift in evaluation

criterion is attributed to the harsh response time requirements of FFR services, which mandate a response time of 1-2 seconds, in contrast to the more lenient timeframes of 30 seconds and 15 minutes associated with primary and secondary services, respectively. The suitability of ASHP models is assessed from two critical dynamic characteristics of the power response profile: the normalized transient shape and steady-state gain. Moreover, given the variability in working conditions of ASHP systems, specifically fluctuations in air and return water temperatures within specific permissible ranges, it is essential to demonstrate the model's suitability based on an assumption of uncertain working conditions.

We simulate the proposed model for ramping and step responses at four working conditions. In the ramping scenario, the resulting close-to-linear response (Fig. 7a) is similar to what we observed from our commercial ASHP (Fig. 2), which can still be described by traditional models as the response differences between diverse working conditions are negligible. However, in the step response simulation, the proposed model shows strong non-linearity that significantly exceeds the capability of traditional models (Fig. 7b). Table III summarizes the performance differences between traditional models and the proposed model under diverse demand-side response scenarios. Based on the presented results, it is apparent that the proposed model provides better insights for the target HSDSR controller design application.

B. PHIL results

In this subsection, we aim to show the PHIL emulation results of the virtual heat pump system in our CoSES laboratory. The overall model is deployed with the computation frequencies mentioned in the last section on our PXIe-8880 system, which has Intel(R) Xeon(R) E5-2618L as CPU at 2.30 GHz and 3 GB of RAM. The actual loop duration to finish every computation iteration is shown in Fig. 8a for the electrical subsystem and Fig. 8b for the thermal subsystem in a one-minute test, where stepping on the modulation input is also applied. With an averaged CPU load of 24% and 0.5 GB of RAM usage, the electrical subsystem has an average loop time of roughly 8.42 us (< 9% of target), while the thermal subsystem has an average of 2296.8 us (< 46% of target). These results indicate a stable real-time operation on the PXIe system, making it eligible for our emulation purposes.

The comparison between the theoretical and experimental current waveform in the time domain is shown in Fig. 9a. We can roughly see that the two waveforms are in similar shapes but with a short delay caused by the Egston CSU internal control system processing. To identify the error, the model output $i^*_{g,abc}$ and experimental result $i_{g,abc}$ are plotted in the frequency domain, as shown in Fig. 9b. We see that the CSU current $i_{g,abc}$ results in an error as the CSU cannot perfectly track the requested current waveform $i^*_{g,abc}$, and most error is on higher order harmonics such as 5th (35%), 15th (24%), 9th (13%), and 11th (12%). The error can be diverse in other laboratories depending on the tracking speed of the used PHIL hardware.

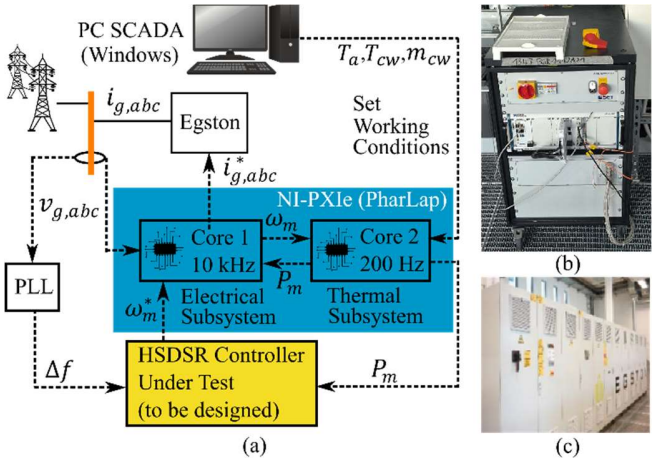

Fig. 6. PHIL emulation of a virtual heat pump for HSDSR design: (a) Setup illustration; (b) NI-PXIe-8880 real-time simulator; (c) Egston CSU;

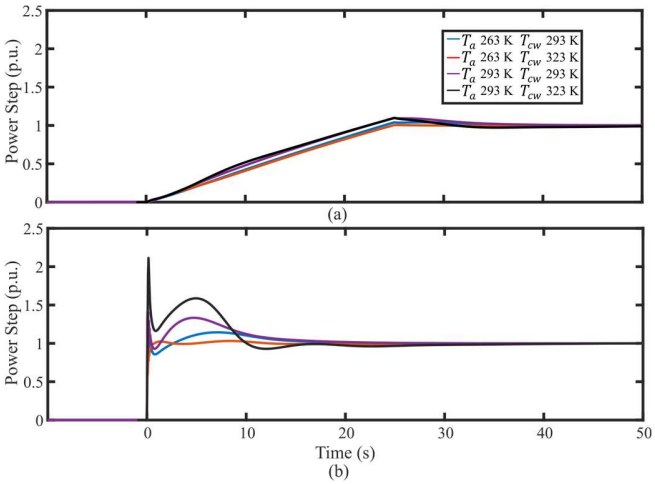

Fig. 7. Speed-power response simulation result of the proposed model at different working conditions (normalized), modulation changing from 50%-100%: (a) via a 25s ramp; (b) via a sudden step.

TABLE III. THE PROPOSED ASHP MODEL V.S. TRADITIONAL ASHP MODELS IN TERMS OF POWER RESPONSE (FOR UNCERTAIN WORKING CONDITIONS)

	Step response (HSDSR)	Ramp response (30s)	Ramp response (mins)
Quasi-static models [18][19]	Tran.: Mismatch S.S.G: Accurate	Tran.: Mismatch S.S.G: Accurate	Tran.: Accurate S.S.G: Accurate
Constant transfer function/state-space models [20][21]	Tran.: Mismatch S.S.G: Mismatch	Tran.: Accurate S.S.G: Mismatch	Tran.: Accurate S.S.G: Mismatch
Hammerstein-Wiener models [8][22]	Tran.: Mismatch S.S.G: Accurate	Tran.: Accurate S.S.G: Accurate	Tran.: Accurate S.S.G: Accurate
Proposed model	Tran.: Accurate S.S.G: Accurate	Tran.: Accurate S.S.G: Accurate	Tran.: Accurate S.S.G: Accurate

* Tran.: normalized transient shape; S.S.G: steady-state gain;

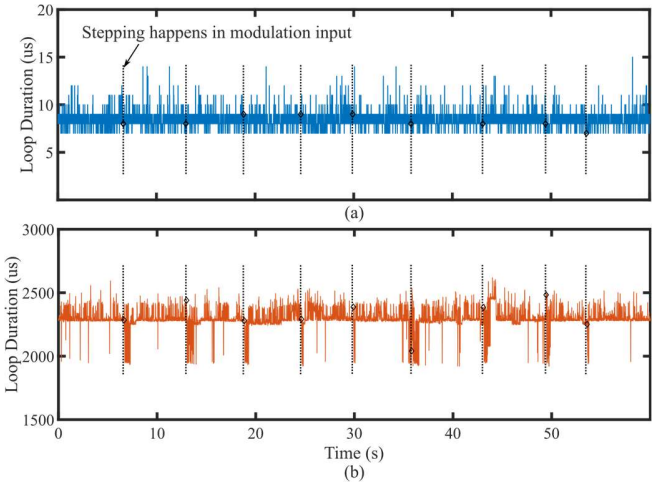

Fig. 8. Actual time to finish one computation step: (a) electrical subsystem; (b) thermal subsystem.

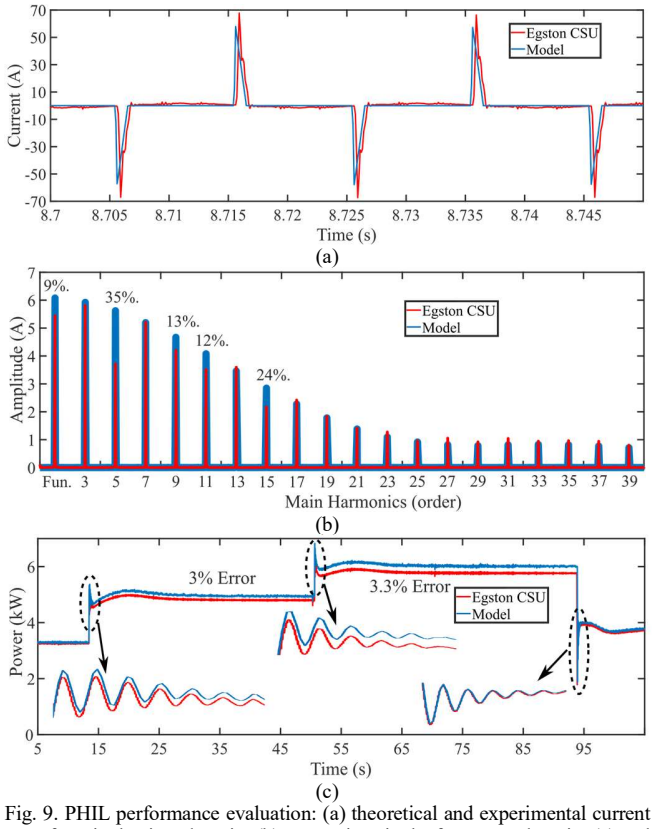

Fig. 9. PHIL performance evaluation: (a) theoretical and experimental current waveform in the time domain; (b) comparison in the frequency domain; (c) real power profile comparison in a modulation period;

We then evaluate the ASHP PHIL system performance during a modulation stepping period and check whether the PHIL system can reproduce the real power profile calculated by the real-time simulator, as shown in Fig. 9c. It is evident that the PHIL system matches the model output with a specific steady-state error, caused by the CSU imperfect current tracking. These problems should be tackled with an equipment-specific compensation factor to adjust the $i^*_{g,abc}$ sent to the hardware. However, we also note that the PHIL system's speed-power transient characteristics are well preserved.

V. Conclusions

This paper identified a gap in ASHP modeling literature that is generally unsuitable for FFR applications in ADG. We proposed a way to simulate the physical non-linear behavior of ASHP during rapid modulation and provide PHIL emulation results. Our model uses existing methods in electrical and mechanical engineering fields to develop a standard physics-based non-linear model that can apply to most distributed ASHPs via parameter tuning. The model was tested with one set of parameters and deployed in the CoSES laboratory PHIL environment. The results suggest that the PHIL experiment can demonstrate the target non-linear behavior on a real active distribution grid with an acceptable real-time computational burden. Our model can be used to mitigate thermal equipment insufficiency in power system laboratories, which generally possess a real-time simulator with PHIL capabilities.

Acknowledgment

Ruihao Song is supported by the Bavarian Research Foundation through the project "Sector coupling und Microgrids (STROM, AZ-1473-20)". Dr. Vedran S. Perić is supported by Deutsche Forschungsgemeinschaft (DFG) through the project "Optimal Operation of Integrated Low-Temperature Bidirectional Heat and Electric Grids (IntElHeat, 450821044)".

References

[1] International Energy Agency, "The future of heat pumps." [Online]. Available: https://www.iea.org/reports/the-future-of-heat-pumps

[2] R. Song, T. Hamacher, V. Terzija, and V. S. Perić, "Potentials of using electric-thermal sector coupling for frequency control: A review," *Int. J. Electr. Power Energy Syst.*, vol. 151, p. 109194, Sep. 2023, doi: 10.1016/j.ijepes.2023.109194.

[3] Y.-J. Kim and J. Wang, "Power Hardware-in-the-Loop Simulation Study on Frequency Regulation Through Direct Load Control of Thermal and Electrical Energy Storage Resources," *IEEE Trans. Smart Grid*, vol. 9, no. 4, pp. 2786–2796, Jul. 2018, doi: 10.1109/TSG.2016.2620176.

[4] A. Spina *et al.*, "Smart Grid Technology Lab – A Full-Scale Low Voltage Research Facility at TU Dortmund University," in *2018 AEIT International Annual Conference*, IEEE, Oct. 2018, pp. 1–6. doi: 10.23919/AEIT.2018.8577378.

[5] G. De Carne and D. Kottonau, "Power Hardware In the Loop laboratory testing capability for energy technologies," in *2022 AEIT International Annual Conference (AEIT)*, IEEE, Oct. 2022, pp. 1–5. doi: 10.23919/AEIT56783.2022.9951766.

[6] A. Mohapatra, T. Hamacher, and V. S. Peric, "PHIL Infrastructure in CoSES Microgrid Laboratory," in *2022 IEEE PES Innovative Smart Grid Technologies Conference Europe (ISGT-Europe)*, IEEE, Oct. 2022, pp. 1–6. doi: 10.1109/ISGT-Europe54678.2022.9960295.

[7] W. Meesenburg, W. B. Markussen, T. Ommen, and B. Elmegaard, "Optimizing control of two-stage ammonia heat pump for fast regulation of power uptake," *Appl. Energy*, vol. 271, no. April, p. 115126, Aug. 2020, doi: 10.1016/j.apenergy.2020.115126.

[8] Y.-J. Kim, L. K. Norford, and J. L. Kirtley, "Modeling and Analysis of a Variable Speed Heat Pump for Frequency Regulation Through

Direct Load Control," *IEEE Trans. Power Syst.*, vol. 30, no. 1, pp. 397–408, Jan. 2015, doi: 10.1109/TPWRS.2014.2319310.

[9] B. P. Rasmussen, "Dynamic modeling for vapor compression systems—Part I: Literature review," *HVAC&R Res.*, vol. 18, 2012, doi: 10.1080/10789669.2011.582916.

[10] B. P. Rasmussen and A. G. Alleyne, "Control-Oriented Modeling of Transcritical Vapor Compression Systems," *J. Dyn. Syst. Meas. Control*, vol. 126, no. 1, pp. 54–64, Mar. 2004, doi: 10.1115/1.1648312.

[11] O. Ibrahim, F. Fardoun, R. Younes, and H. Louahlia-Gualous, "Air source heat pump water heater: Dynamic modeling, optimal energy management and mini-tubes condensers," *Energy*, vol. 64, pp. 1102–1116, 2014, doi: 10.1016/j.energy.2013.11.017.

[12] V. S. Peric *et al.*, "CoSES Laboratory for Combined Energy Systems At TU Munich," in *2020 IEEE Power & Energy Society General Meeting (PESGM)*, IEEE, Aug. 2020, pp. 1–5. doi: 10.1109/PESGM41954.2020.9281442.

[13] R. C. Portillo *et al.*, "Modeling Strategy for Back-to-Back Three-Level Converters Applied to High-Power Wind Turbines," *IEEE Trans. Ind. Electron.*, vol. 53, no. 5, pp. 1483–1491, Oct. 2006, doi: 10.1109/TIE.2006.882025.

[14] C. Wu, Z. Xingxi, and D. Shiming, "Development of control method and dynamic model for multi-evaporator air conditioners (MEAC)," *Energy Convers. Manag.*, vol. 46, no. 3, pp. 451–465, Feb. 2005, doi: 10.1016/j.enconman.2004.03.004.

[15] A. Outtagarts, P. Haberschill, and M. Lallemand, "The transient response of an evaporator fed through an electronic expansion valve," *Int. J. Energy Res.*, vol. 21, no. 9, pp. 793–807, Jul. 1997, doi: 10.1002/(SICI)1099-114X(199707)21:9<793::AID-ER297>3.0.CO;2-P.

[16] S. Bendapudi, J. E. Braun, and E. A. Groll, "A comparison of moving-boundary and finite-volume formulations for transients in centrifugal chillers," *Int. J. Refrig.*, vol. 31, no. 8, pp. 1437–1452, Dec. 2008, doi: 10.1016/j.ijrefrig.2008.03.006.

[17] TLK-Thermo GmbH, "TIL-Model library for thermal components and systems." [Online]. Available: https://www.tlk-thermo.com/index.php/en/til-suite

[18] F. Fardoun, O. Ibrahim, and A. Zoughaib, "Quasi-Steady State Modeling of an Air Source Heat Pump Water Heater," *Energy Procedia*, vol. 6, pp. 325–330, 2011, doi: 10.1016/j.egypro.2011.05.037.

[19] B. Shen, K. Nawaz, V. Baxter, and A. Elatar, "Development and validation of quasi-steady-state heat pump water heater model having stratified water tank and wrapped-tank condenser," *Int. J. Refrig.*, vol. 87, pp. 78–90, Mar. 2018, doi: 10.1016/j.ijrefrig.2017.10.023.

[20] T. B. Harild Rasmussen, Q. Wu, and M. Zhang, "Primary frequency support from local control of large-scale heat pumps," *Int. J. Electr. Power Energy Syst.*, vol. 133, no. May, p. 107270, Dec. 2021, doi: 10.1016/j.ijepes.2021.107270.

[21] T. B. H. Rasmussen, Q. Wu, J. G. Moller, and M. Zhang, "MPC Coordinated Primary Frequency Support of Small- and Large-Scale Heat Pumps," *IEEE Trans. Smart Grid*, vol. 13, no. 3, pp. 2000–2010, May 2022, doi: 10.1109/TSG.2022.3148601.

[22] R. Song, G. Yon, T. Hamacher, and V. S. Peric, "Data-Driven Model Reduction of the Moving Boundary Heat Pump Dynamic Model," in *2022 IEEE Power & Energy Society General Meeting (PESGM)*, IEEE, Jul. 2022, pp. 1–5. doi: 10.1109/PESGM48719.2022.9916823.

APPENDIX

Model equations of the electrical subsystem [11]

Rectifier (Diode)	$v_{rec}^{+} = \max(v_{g,a}, v_{g,b}, v_{g,c})$, $v_{rec}^{-} = \min(v_{g,a}, v_{g,b}, v_{g,c})$, $i_{g,abc}^{*} = i_{rec}^{+} g_{rec,abc}^{+} + i_{rec}^{-} g_{rec,abc}^{-}$, $g_{rec,a}^{+} = \begin{cases} 1 & v_{g,a} > v_{g,b} \cap v_{g,a} > v_{g,c} \\ 0 & else \end{cases}$, $g_{rec,a}^{-} = \begin{cases} 1 & v_{g,a} < v_{g,b} \cap v_{g,a} < v_{g,c} \\ 0 & else \end{cases}$.
Dc filter (RC)	$R_f i_{rec}^{\pm} = v_{rec}^{\pm} - v_{dc}^{\pm}$, $i_{rec}^{+} \geq 0$, $i_{rec}^{-} \leq 0$, $C_f \frac{dv_{dc}^{\pm}}{dt} = i_{rec}^{\pm} - i_{dc}^{\pm}$.
Inverter and Control (Three-level, V/f)	$v_{s,abc} = \frac{1}{2} g_{i,abc}^{+} v_{dc}^{+} + \frac{1}{2} g_{i,abc}^{-} v_{dc}^{-}$, $i_{dc}^{+} = \frac{1}{2}(g_{i,a}^{+} i_{s,a} + g_{i,b}^{+} i_{s,b} + g_{i,c}^{+} i_{s,c})$, $i_{dc}^{-} = \frac{1}{2}(g_{i,a}^{-} i_{s,a} + g_{i,b}^{-} i_{s,b} + g_{i,c}^{-} i_{s,c})$, $g_{i,abc}^{+} = -g_{i,abc}^{-}$, $f = k_p(\omega_m^{*} - \omega_m) + k_i \int (\omega_m^{*} - \omega_m)\, dt$, $g_{i,a}^{+} = \frac{k_\varphi f sin(2\pi f)}{\bar{v}_{dc}}$.
Machine (squirrel-cage induction machine)	$\frac{d\varphi_{s,q}}{dt} = v_{s,q} - R_s i_{s,q} - \omega_e \varphi_{s,d}$, $\frac{d\varphi_{s,d}}{dt} = v_{s,d} - R_s i_{s,d} + \omega_e \varphi_{s,q}$, $\frac{d\varphi'_{r,q}}{dt} = v'_{r,q} - R'_r i'_{r,q}$, $\frac{d\varphi'_{r,d}}{dt} = v'_{r,d} - R'_r i'_{r,d}$, $\varphi_{s,q} = (L_{l,s} + L_{mg}) i_{s,q} + L_{mg} i'_{r,q}$, $\varphi_{s,d} = (L_{l,s} + L_{mg}) i_{s,d} + L_{mg} i'_{r,d}$, $\varphi'_{r,q} = (L'_{l,r} + L_{mg}) i'_{r,q} + L_{mg} i_{s,q}$, $\varphi'_{r,d} = (L'_{l,r} + L_{mg}) i'_{r,d} + L_{mg} i_{s,d}$, $J \frac{d\omega_m}{dt} = T_e - k_F \omega_m - T_{load}$, $T_e = 1.5p(\varphi_{s,d} i_{s,q} + \varphi_{s,q} i_{s,d})$, $T_{load} = \frac{P_m}{\omega_m}$

- **Variables:** v: Voltage; i: Current; g: Gate-equivalent function; R: Resistance; C: Capacitance; ω: Rotational speed; φ: Flux; L: Inductance; p: Pole-pairs; T:Torque; J: Moment of inertia; f: Frequency; k: Constants.
- **Subscripts:** g: Grid; rec: Rectifier; f: Filter; i: Inverter; m: Mechanical; e: Electrical; c: Cross-section; s: Stator; r: Rotor; mg: Magnetizing; F: Friction; ls: Leakage.
- **Superscripts:** $*$: Reference; $'$: Referred to the stator side; $+/-$: Variable polarity.

Model equations of the thermal subsystem [6]

Eva.	Mass Conservation	Energy Conservation (refrigerant)	Energy Conservation (wall)
Two-phase zone (1^{st})	$\left(\frac{d\rho'_v}{dp}\bar{\gamma} + \frac{d\rho'_l}{dp}(1-\bar{\gamma})\right) A_{i,c} L_{tp} \frac{dp}{dt} + \dot{m}_b - \dot{m}_{in}$ $+(\rho'_l - \rho'_v)(1-\bar{\gamma}) A_{i,c} \frac{dL_{tp}}{dt} = 0.$	$\left(\left(\frac{d\rho'_v}{dp} h_v + \frac{dh'_v}{dp}\rho_v\right)\bar{\gamma} + \left(\frac{d\rho'_l}{dp} h_l + \frac{dh'_l}{dp}\rho_l\right)(1-\bar{\gamma}) - 1\right)$ $A_{i,c} L_{tp} \frac{dp}{dt} + (\rho_l h_l - \rho_v h_v)(1-\bar{\gamma}) A_{i,c} \frac{dL_{tp}}{dt} + \dot{m}_b h_b$ $-\dot{m}_{in} h_{in} = A_{i,s} \frac{L_{tp}}{L_t} \alpha_{i,tp} (T_{w1} - T_{r1}).$	$A_{i,s} \frac{L_{tp}}{L_t} \alpha_{i,tp} (T_{r,tp} - T_{w,tp})$ $+ A_{o,s} \frac{L_{tp}}{L_t} \alpha_o (T_a - T_{w,tp})$ $= C_w \rho_w (A_{o,c} - A_{i,c}) L_{tp} \frac{dT_{w,tp}}{dt}.$
Vapor zone (2^{nd})	$\left(\frac{\partial \rho_v}{\partial p}\Big\|_{h_v} + \frac{1}{2}\frac{\partial \rho_v}{\partial h_v}\Big|_p \frac{dh'_v}{dp}\right) A_{i,c} L_v \frac{dp}{dt} + \dot{m}_{out} - \dot{m}_b$ $+(\rho'_v - \rho_v) A_{i,c} \frac{dL_{tp}}{dt} + \frac{1}{2}\frac{\partial \rho_v}{\partial h_v}\Big|_p A_{i,c} L_v \frac{dh_{out}}{dt} = 0.$	$A_{i,c} L_v \frac{dp}{dt}\left(\left(\frac{\partial \rho_v}{\partial p}\Big\|_{h_v} + \frac{1}{2}\frac{\partial \rho_v}{\partial h_v}\Big|_p \frac{dh'_v}{dp}\right) h_v + \frac{1}{2}\frac{dh'_v}{dp}\rho_v - 1\right)$ $+\frac{1}{2}\left(\frac{\partial \rho_v}{\partial h_v}\Big|_p h_v + \rho_v\right) A_{i,c} L_v \frac{dh_{out}}{dt} + \dot{m}_{out} h_{out} - \dot{m}_b h_b$ $+(\rho'_v h'_v - \rho_v h_v) A_{i,c} \frac{dL_{tp}}{dt} = A_{i,s} \frac{L_v}{L_t} \alpha_{i,v} (T_{w,v} - T_{r,v}).$	$C_w \rho_w (A_{o,c} - A_{i,c}) L_v$ $\left(\frac{dL_{tp}}{dt}\frac{T_{w,tp} - T_{w,v}}{L_v} + \frac{dT_{w,v}}{dt}\right)$ $= A_{i,s} \frac{L_v}{L_t} \alpha_{i,v} (T_{r,v} - T_{w,v})$ $+ A_{o,s} \frac{L_v}{L_t} \alpha_o (T_a - T_{w,v}).$

Con.	Mass Conservation	Energy Conservation (refrigerant)	Energy Conservation (wall)	Energy Conservation (water)
Vapor zone	…	…	…	$C_{cw} \rho_{cw} V_{cw} \frac{dT_{hw}}{dt} = A_{o,s} \frac{L_v}{L_t} \alpha_o (T_{w,v} - T_{hw})$ $+ A_{o,s} \frac{L_{tp}}{L_t} \alpha_o (T_{w,tp} - T_{hw}) + \dot{m}_{cw} C_{cw} (T_{cw} - T_{hw})$
Two-phase zone	…	…	…	

Comp.	$P_m = \underbrace{\left(\frac{\omega_m}{2\pi} V_{comp} \rho_{in} \eta\right)}_{MassFlow} \underbrace{\left(\frac{k_1 R T_{in}}{k_1 - 1}\left(\left(\frac{p_{out}}{p_{in}}\right)^{\frac{k_1 - 1}{k_1}} - 1\right)\right)}_{\Delta h}$
Exp. Valve	$\dot{m}_{out} = A_{ori} k_{ev} \sqrt{\rho_{in}(p_{out} - p_{in})}$ $A_{ori} = k_3 (T^{*}_{sh} - T_{sh}) + k_4 \int (T^{*}_{sh} - T_{sh}) dt + A_{base}$

- **Abbreviations**: Eva. = Evaporator; Con. = Condenser; Comp. = Compressor; Exp. = Expansion.
- **Variables:** ρ: Density; p: Pressure; h: Specific enthalpy; $\dot{m}$: Massflow; $\bar{\gamma}$: Average vapor fraction; A: Cross-section area; L: Zone length; α: Heat transfer coefficient; C: Specific heat; T: Temperature; P: Power; V: Volume; ω: Speed; η: Efficiency; R: Gas constant; k: Constants.
- **Subscripts**: v: Vapor; l: Liquid; c: Cross-section; s: Surface; i/o: Inner/Outter; t: Total; tp: Two-phase zone; r: refrigerant; w: Wall; a: Air; b: Boundary between two-phase and vapor zone; in/out: Input/Output; cw: Cold water; hw: Hot water; sh: Superheat, ori: Orifice.
- **Superscripts**: $*$: Reference; $'$: Variables in saturation state.